EFFECT OF SHELL TEMPERATURE IN THERMAL CONTROL SOLIDIFICATION PROCESS ON MICROSTRUCTURE AND STRESS RUPTURE PROPERTY OF CAST EQUIAXED SUPERALLOY

Guoqiang Cao[1], Yuqiao Shen[1], Gang Li[2], Wenya Peng[2]
[1]School of Mechanical and Electrical Engineering, Shenyang Aerospace University, P.R. China;
[2]AECC Hunan Aviation Powerplant Research Institute, P.R. China
sycgq@126.com

Abstract. Cast equiaxed superalloy is commonly used in the manufacture of engine turbine blades and complex structural castings due to its excellent casting properties and comprehensive mechanical properties. The more adaptable thermal control solidification process is usually used to refine the equiaxed crystal structure. In this paper, the microstructure and fracture surface of this alloy after solid solution were observed and characterized by means of OM, SEM, and EDS, and the effects of thermally controlled solidification processes with different shell temperatures on the microstructure and stress fracture properties of this alloy were investigated. The results showed that in this cast equiaxed crystal alloy, increasing the shell temperature from 1300 ºC to 1330 ºC causes the grain size to grow, microporosity to significantly decrease, and eutectic content and size to slightly increase. Both S1 and S2 alloys formed MC and M_6C carbides after solid solution treatment. The size and content of carbides increased as the shell temperature rose, whereas the size and content of the γ' phase decreased. As the shell temperature increases, the stress rupture properties increase slightly, while the degree of rafting increases dramatically. Cracks are mainly formed at the aggregation of microporosity, eutectics, and carbides. The reasons why cracks occur in the two alloys can differ. This study provides guidance for the design of a thermal control solidification process for cast equiaxed superalloys.

Key words: cast equiaxed superalloy, thermal control solidification process, shell temperature, stress rupture property.

Introduction

Nickel-based superalloys are the material of first choice for hot end components in the aerospace field due to their excellent properties of high strength, creep resistance, fatigue resistance, oxidation resistance, and corrosion resistance [1]. The alloy chosen for this work is a typical high-W cast equiaxed superalloy, which has excellent high temperature characteristics and is often used in turbine blades, turbine guiding vanes, and other high temperature structural parts [2].

The thermal control method is a fine-grained casting process that increases the cooling rate during the solidification of the casting by controlling the withdrawal rate, pouring temperature, shell temperature, and other process parameters, thus increasing the undercooling degree to raise the nucleation rate [3-4]. As the G/R ratio at the solid/liquid interface front in the thermal control solidification process must be tightly controlled within the equiaxed crystal region, the control requirement of the solidification process is much more demanding than that of directional and single crystal casting technology [5]. It has been shown that the thermal control process may be used to manufacture large cast steel components in addition to small precision castings [6]. Wu et al. studied the secondary dendrite arm spacing, microporosity, and density characteristics of the thermal control solidification K424 alloy and demonstrated the differences between the K424 alloy and conventional casting alloys in these properties [7].

In the thermal control process, the shell temperature lies between the solid and liquid phase lines of the alloy. Changes in the shell temperature can lead to variations in the cooling rate, which can enhance the casting's filling capacity and prevent the thin wall and big size effects. Tao et al. investigated the impact of various shell preheating temperatures on the microstructure and mechanical characteristics of IN738LC alloy [8]. Xue et al. investigated the effect of two shell temperatures, 1500 ºC and 1540 ºC, on the microstructure of typical cross-sections of the blade [9]. None of the above studies mentioned the role of shell temperature on the microstructure and the stress rupture property during the thermal control process for the preparation of equiaxed high temperature alloys. Therefore, it is necessary to investigate the evolution of the solidification behaviour of equiaxed high temperature alloys at different shell temperatures.

In this paper, the effects of two shell temperatures on the equiaxed crystal organization of the alloy are investigated, and the grain size, microporosity, γ/γ' eutectic, carbide, γ' and persistence properties

of the alloy are analyzed. The link between the microstructure and stress rupture property, as well as the inherent correlation between the shell temperature and microstructure, are discussed. This research offers a trial guide for using this alloy in real-world manufacturing.

Materials and methods

A cast equiaxed crystal high temperature alloy developed by the Beijing Institute of Aeronautical Materials is used as the test alloy, and its nominal composition (mass fraction) is shown in Table 1. Thermal control process tests on the alloy test bars were performed using a vacuum induction directional solidification furnace. Each set of shells contained eight test bars that were the size of a Φ14 x 160 mm test bar. The shells were heated in heaters with the same upper and lower heater temperatures, both with a withdrawal rate of 15 mm/min, both with a casting temperature of 1400 ºC and shell temperatures of 1300 ºC and 1330 ºC, respectively. The alloy numbers were S1 and S2.

Table 1

Nominal chemical composition of the alloy (mass fraction/%)

Ni	W	Co	Cr	Al	Ti	Mo	Nb	C
Bal.	10.2	10.0	8.5	5.7	2.5	1.8	1.1	0.15

Following casting, two groups of test bars were given a solution treatment under vacuum with a heat treatment regime of 1210 ºC/4h and cooled in air. The cross-section was measured at the same location in the middle of the two test bars after one test bar was randomly chosen from each group. A typical metallographic preparation process was used to prepare the samples. Corrosion was accomplished using a corrosive solution of $HF:HNO_3:CH_3COOH:H_2O = 1:33:33:33$. The grain morphology was investigated with a Leica M205C body microscope. The microporosity and dendritic morphology were investigated using a DM4000M optical microscope (OM). The microstructure of the alloy was characterized using a ZEISS SUPRA 55 field emission scanning electron microscope (SEM). Image-Pro Plus software was used to calculate the parameters.

After heat treatment, the rods were then transformed into samples for a stress rupture property test with a 5mm diameter and 25mm length. The 975 ºC/225MPa test conditions were used. Following the test, SEM was utilized to characterize the fracture morphology and microstructure of the two samples and to assess the impact of the shell temperature on the performance of the stress rupture property.

Results and discussion

The grain morphology of the alloys at various shell temperatures is shown in Figure 1. When the shell temperature is raised from 1300 ºC to 1330 ºC, the alloy's average grain size increases noticeably while maintaining its typical dendritic structure. S1 has about 15 grains, nearly all of which are equiaxed, and S2 has about 7 grains and may contain a few columnar grains, cutting the number of grains in half. During solidification, an increase in the shell temperature leads to a decrease in the cooling rate of the alloy liquid and a decrease in the nucleation ability of the shell surface, resulting in a decrease in the nucleation rate, a larger grain size, and a decrease in the number of grains. The higher shell temperature causes a difference in the cooling rate between the casting surface and the centre of the casting, which may result in the formation of columnar crystals that grow from the outside to the inside [10]. In addition, the increase in the shell temperature will make the grains coarser and the tissue uniformity worse.

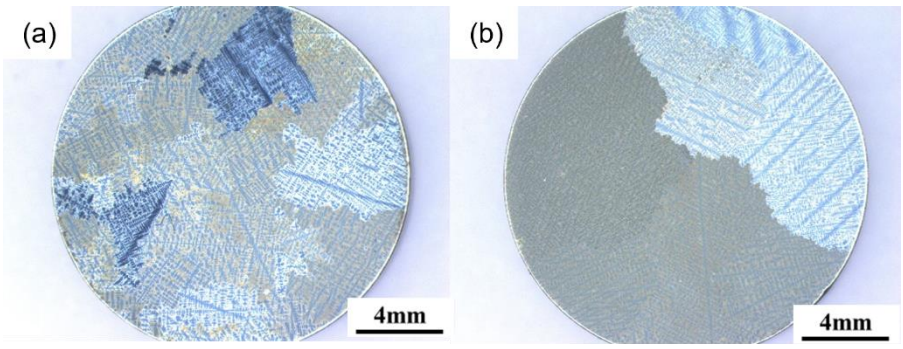

Fig. 1. **Grain morphology at different shell temperatures:** a – alloy S1; b – alloy S2

The microporosity of the alloys at different shell temperatures is shown in Fig. 2. When the shell temperature increases, the microporosity decreases significantly, and the average microporosity of S1 and S2 is 0.42 ± 0.2% and 0.15 ± 0.05%, respectively. Compared with S2, the microscopic sparseness of S1 is larger in size and mostly concentrated at grain boundaries or interdendritic regions. There is enough residual alloying liquid between the dendrites to make up the shrinkage through the capillaries during solidification [5]. When the shell temperature is low, there is less alloying fluid involved, and the capillary channels are blocked, preventing complementary shrinkage, so an increase in the shell temperature results in less microporosity.

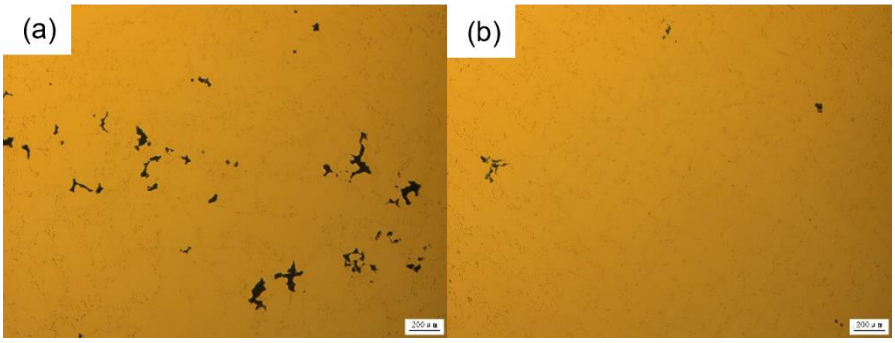

Fig. 2. **Microporosity at different shell temperatures:** a – alloy S1; b – alloy S2

Figure 3 shows the γ/γ' eutectic morphology of the alloy at different shell temperatures. Statistically, the two alloys have an average percentage of 1.9 ± 0.5% and 2.7 ± 0.5%, respectively. When the shell temperature rises, the eutectic content and size both slightly increase. Eutectic is also distributed in the form of a sunflower in the interdendritic regions or at grain borders. The γ' phase forming elements such as Al, Ti, Nb, and Ta have a large solubility in the γ' phase, and these elements deviate toward the interdendrites and precipitate as eutectic when the liquid metal between the dendrites reaches the composition of eutectic [11-12]. The degree of segregation and the amount of remaining liquid phase between the dendrites rise with increasing the shell temperature, which also marginally increases the size and content of the eutectic.

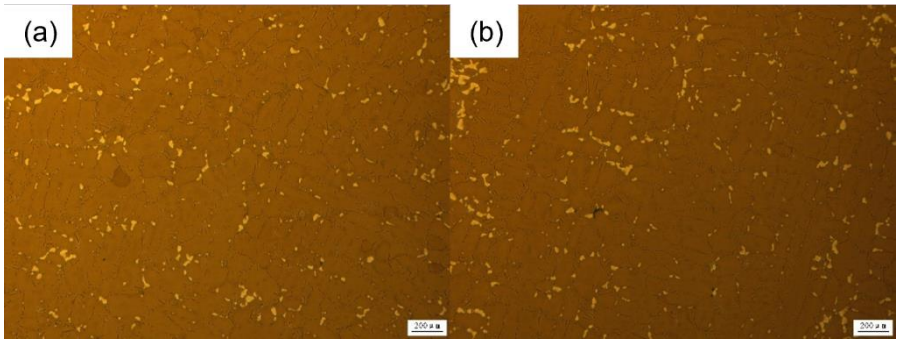

Fig. 3. **γ/γ' eutectic morphology at different shell temperatures:** a – alloy S1; b – alloy S2

Figure 4 shows the SEM morphology of the alloys at various shell temperatures. According to the image, the interdendritic region or grain boundaries of both alloys exhibit microporosity and eutectic along with a sizable quantity of lined white and off-white massive or skeletal carbides. Statistics show that S1 and S2 had average carbide contents of 0.66 ± 0.09% and 0.75 ± 0.12%, respectively. The carbides somewhat increase as the shell's temperature rises. Figure 5 shows how the EDS analysis confirms that the lining degree is white in the form of granular or lumpy forms as M_6C-type carbides, while the lining degree is greyish-white in the form of large lumps or skeletal forms as MC-type carbides, rich in Ti and Nb elements and dissolved in some Mo and W elements. Both S1 and S2 alloys are solid solution treated; therefore, MC-type and M_6C-type carbides exist. During solid solution treatment, MC-type carbides often undergo breakdown to generate M_6C carbides. The S2 alloy has more carbides and is bigger than the S1 alloy due to the greater segregation of alloying elements caused by the rise in shell temperature [13].

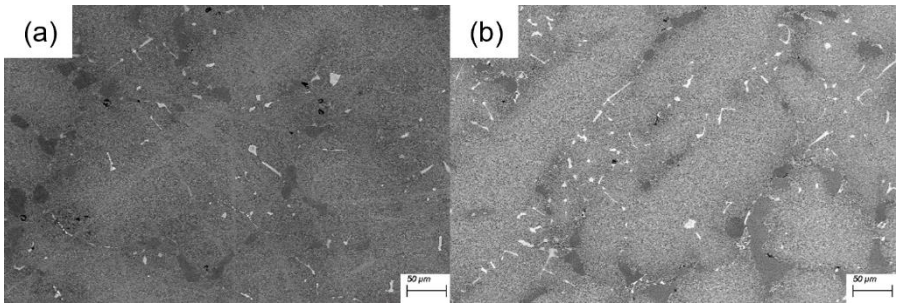

Fig. 4. **SEM images at different shell temperatures:** a – alloy S1; b – alloy S2

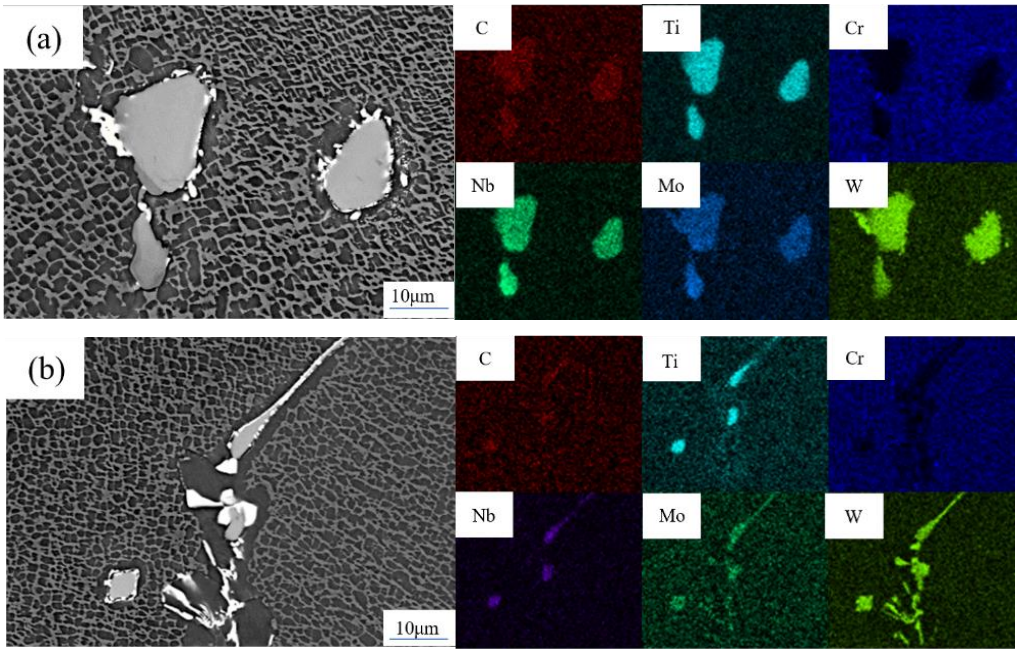

Fig. 5. **Carbide morphology and composition at different shell temperatures:** a – alloy S1; b – alloy S2

Figure 6 shows the γ' morphology of the interdendritic region of the alloys at different shell temperatures. After solid solution treatment, the γ' phases of both alloys are irregularly cubic, and a small amount of secondary γ' phases exist in the middle of the γ matrix. Statistically, the average size of the γ' phase of S1 and S2 alloys were 142.3 ± 4.7 mm and 151.4 ± 5.1 mm, respectively, and the area fraction of the γ' phase was 49.6 ± 2.2% and 48.7 ± 3.4%, respectively. With rising shell temperature, the average size of the γ' phase shrinks significantly while the γ' content nearly stays constant. The size of the γ' phase is relatively small, but the content is practically constant, since as the shell temperature rises, the temperature gradient at the solid-liquid interface front will also rise. This will promote precipitation and nucleation but hinder the expansion of the γ' phase [14].

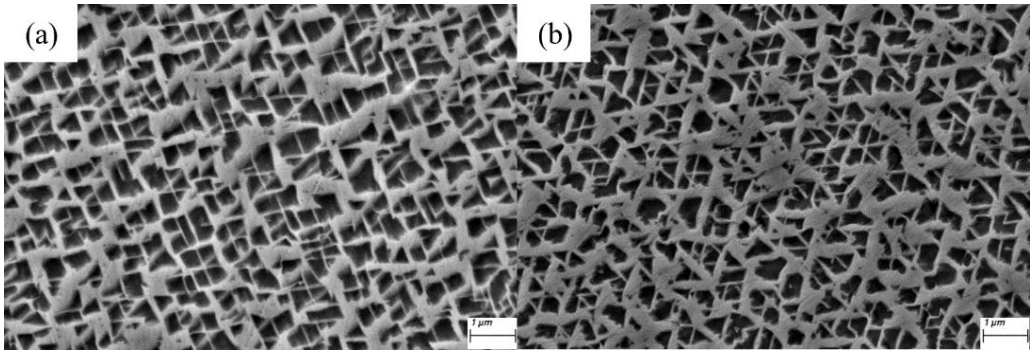

Fig. 6. **γ/γ' eutectic morphology at different shell temperatures:** a – alloy S1; b – alloy S2

Table 2 shows the stress rupture property of the alloy at 975 ºC/225 MPa for different shell temperatures. When the shell temperature is increased from 1300 ºC to 1330 ºC, the rupture life increases from 5.60 h to 17.5 h, the elongation increases from 1.96% to 1.88%, and the section reduction increases from 2.39% to 3.57%. Figure 7 shows the rafting of the γ' phase at the fracture of the alloy at different shell temperatures. As the shell temperature increases, the degree of rafting increases significantly, and the γ' phase of the S1 alloy has formed a complete rafting structure. Figure 8 shows the grain boundary secondary crack pattern of the alloy at different shell temperatures. The cracks are focused on microporosity, γ/γ' eutectic and carbide aggregation, and extend along interdendritic or grain boundaries. Under early high temperature stress conditions, cracks in the S1 alloy may develop between the microporosity, whereas cracks in the S2 alloy stretch along the carbide, eutectic, and other impurity phases [15]. S1 has more microporosity at lower shell temperatures, whereas S2 has more carbide and eutectic content at higher shell temperatures. Therefore, the possible causes of fracture are different for the two alloys, but both occur at the interdendritic or grain boundaries where microporosity, γ/γ' eutectic, and carbide are more concentrated.

Table 2

Stress rupture property with different shell temperature at 975 ºC/225MPa

Alloy	Rupture life (h)	Elongation (%)	Reduction (%)
S1	5.60	1.96	2.39
S2	17.5	1.88	3.57

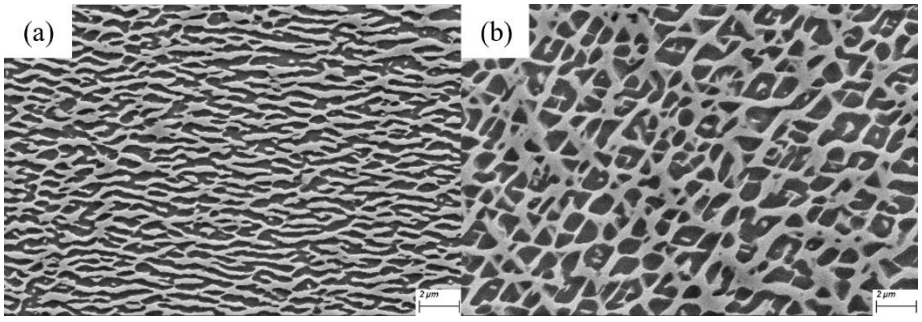

Fig. 7. **γ' phase rafting at the fracture at different shell temperatures:**
a – alloy S1; b – alloy S2

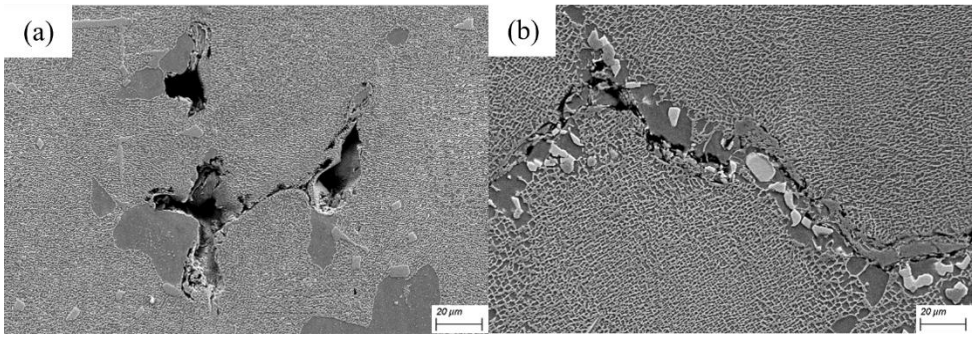

Fig. 8. **Grain boundary secondary cracking pattern at different shell temperatures:**
a – alloy S1; b – alloy S2

Conclusions

1. In this cast equiaxed crystal alloy, increasing the shell temperature from 1300 ºC to 1330 ºC causes the grain size to grow, microporosity to significantly decrease, and eutectic content and size to slightly increase.
2. Both S1 and S2 alloys formed MC and M_6C carbides after solid solution treatment. The size and content of carbides increased as the shell temperature rose, whereas the size and content of the γ' phase decreased.

3. As the shell temperature increases, the stress rupture properties increase slightly, while the degree of rafting increases dramatically. Cracks are mostly formed at the aggregation of microporosity, eutectics, and carbides. The reasons why cracks occur in the two alloys can differ.

Acknowledgements

This work was supported by the Natural Science Foundation of China (Nos. 52001297, 91860202).

Author contributions

Conceptualization, G.C.; methodology, G.C.; validation, G.C. and Y.S.; formal analysis, G.C. and G.L.; investigation, G.C. and W.P.; data curation, G.C.; writing – original draft preparation, G.C.; writing – review and editing, Y.S. and G.C.; visualization, G.L.; project administration, G.C.; funding acquisition, G.C. All authors have read and agreed to the published version of the manuscript.

References

[1] Reed R.C. The superalloys: fundamentals and applications. First edition. New York: Cambridge University Press, 2006. 1 p.
[2] Xiaotong G., Weiwei Z., Chengbo X., et al. Microstructural degradation and tensile properties of K465 equiaxed cast superalloy after short time overheating. Journal of Materials Engineering, vol. 46, 2018, pp. 77-86.
[3] Changxu S, Zengyong Z. China superalloy for 50 years. First edition. Beijing: Metallurgical Industry Press, 2006. 72-81 p.
[4] Ziqi J., Jun Z., Taiwen H., et al. Enhanced grain refinement and porosity control of the polycrystalline superalloy by a modified thermally-controlled solidification. Advanced Engineering Materials, vol 18, 2016, pp.1785-1791.
[5] Jun Z., Ziqi J., Taiwen H., et al. Research and development of equiaxed grain solidification and forming technology for nickel-based cast superalloys. Acta Metallurgica Sinica, vol.55, 2019, pp.1145-1159.
[6] Zhenjiang M., Mingpan M., Zhenan L. Production Practice of Large-size Steel Castings by Using Fine Grain Casting Process (FGCP). Foundry Technology, vol.32, 2011, pp.574-576.
[7] Wu J., Feng D., Li J., et al. Research on the characteristic thermally controlled solidification processed alloy K242. Proceedings of the 11th China Superalloy Annual Conference "High-temperature structural materials for power and energy use", May, 2007, Zengyong Zhong, pp. 332-335.
[8] Fei T., Xiong G., Zhenheng G. Effect of shell mould temperature on microstructure and properties of IN738LC superalloy. Heavy Casting and Forging, vol 2, 2020, pp.9-10.
[9] Yanpeng X., Xiaoguang W., Jinqian Z., et al. Effect of two mould temperature on solidification microstructure of DD9 single crystal turbine blade. Journal of Material Engineering, vol 50, 2022, pp:80-87.
[10] Jie Z., Zhang J., Huang T., et al. Enhanced grain refinement and microporosity control of the polycrystalline superalloy by a modified thermally controlled solidification. Advanced Engineering Materials, vol 18, 2016, pp. 1785-1791.
[11] Tao J., Jinguo L., Nairen Z., et al. Effect of withdrawal rate on solidification parameters and microstructure of a nickel-base single crystal superalloy. Journal of Material Engineering, vol 3, 2002, pp. 36-39 + 48.
[12] Li J., Zhen W., Tao J., et al. Effect of withdrawal rate on microstructure of a nickel-base single crystal superalloy. Materials for Mechanical Engineering, vol 26, 2002, pp. 17-19 + 46.
[13] Zihan M., Junfeng Q., Zhuhuan Y., et al. Effect of drawing rate microstructure and segregation of directionally solidified nickel-based superalloy. Foundry technology, vol 41, 2020, pp. 313-318.
[14] Hua J., Yunfei B., Qing L., et al. Effect of parameters of HRS process on microstructure of DZ466 Ni-based superalloy. Journal of Aeronautical Materials, vol.38, 2018, pp. 52-57.
[15] Shuseng W., Zhiru S., Lufan C., et al. Influence of C contents on microstructure and high temperature stress rupture properties of polycrystalline nickel-based superalloy. Hot Working Technology, vol 51, 2022, pp. 14-19.